LM-05K159
November 14, 2005

First Principles Calculations of Electrochemically Controlled Hydrogen Mobility and Uptake at the Ni(111)H_2O Interface

C Taylor, R Kelly and M Neurock

First principles calculations of electrochemically controlled hydrogen mobility and uptake at the Ni(111)/H_2O interface

Christopher Taylor[1], *Robert G. Kelly*[1], *Matthew Neurock*[2]

[1]Department of Materials Science and Engineering

[2]Department of Chemical Engineering

University of Virginia

Charlottesville, VA 22903

Abstract

The binding of hydrogen on Ni(111) in the presence of an water is considered using both a bilayer and a saturated model of the solvent environment. The presence of a water bilayer did not change the binding energies or geometry of hydrogen on the Ni(111) compared to adsorption in ultra-high vacuum. Using the saturated model (four bilayers over the surface) we also monitored the change in hydrogen binding as a function of electrochemical potential. Binding energies for hydrogen at the hcp and octahedral sites shifted endothermically as the potential was made more anodic, indicating that reductive partial charge transfer occurs. Binding at the tetrahedral site was found to be partially oxidizing. Calculation of vibrational modes allowed the extrapolation of ab initio results to ambient and elevated temperatures. Surface Pourbaix diagrams were constructed illustrating the stability of various phases on the Ni(111) surface as a function of pH and potential.

Introduction

Nickel base alloys are commonly employed in engineering applications due to their high strength and high corrosion resistance. The high affinity of nickel for hydrogen also suggests their utility as hydrogen storage materials, and hydrogenation catalysts. Even in high-purity water the corrosion of such alloys can occur, particularly via stress corrosion cracking (SCC)[1]. In such systems hydrogen is often introduced to create a reducing environment. However, H_2 may dissociatively adsorb (as in UHV[2]) to form surface hydrogen that may be absorbed into the bulk or remain mobile across the surface. Hydrogen embrittlement is one possible explanation for SCC in nickel-base alloys. The other proposed mechanism is dissolution of Ni at the exposed crack tip. Understanding the activity of hydrogen on model nickel surfaces, therefore, is important to problems in both corrosion and electrocatalysis.

Experimental techniques, such as surface enhanced Raman spectroscopy, in situ electron microscopy and crystal rod truncation techniques are now beginning to capture electrochemical processes with atomic resolution[3,4]. There remains, however, a demand for first-principles models that can describe the complex phenomena currently being observed, such as changes in molecular structure[5,6], chemisorption[7,8], water activation[9] and surface reconstruction[10].

Recent theoretical[11] and experimental[2,12-15] explorations of the surface chemistry of hydrogen on metal electrodes have primarily been conducted ex situ, that is, in ultra-high vacuum conditions (UHV). Christmann's low energy electron diffraction (LEED) studies of hydrogen on Ni(111) revealed the formation of an ordered (2x2)-2H hexagonal structure with equal occupation of the hexagonal close packed (hcp) and face centered

cubic (fcc) three-fold hollow sites[2]. The vibrational study by Yanagita et al.[15] shows that hydrogen forms (2x2)-2H island structures on the Ni(111) surface, with no evidence of quantum tunneling effects and vibrational modes at 2.2 THz and 3.1 THz, shifting to 2.8 THz and 3.4 THz at the higher (1x1) coverage. Hammer et al.[12] demonstrated significant surface reconstruction of the Ni(111) surface upon hydrogen adsorption, whereby the nickel atoms directly bonded to hydrogen are lifted out of the plane by 0.04 Å. The kinetics of hydrogen absorption were probed using collision techniques by both Maynard et al.[13] and Wright et al.[14] with activation barriers for resurfacing between 0.4 and 0.5 eV. Maynard et al.[13] also calculated vibrational modes of subsurface hydrogen to be between 2.4 and 2.6 THz.

A number of theoretical studies that consider hydrogen uptake and mobility on the single crystal Ni(111) surface under UHV conditions have been recently published[11,16]. Greeley and Mavrikakis[11] calculated the binding energy of hydrogen at various surface sites on Ni(111) and also determined barriers to first and second layer hydrogen absorption. Hydrogen uptake was shown to be endothermic by 0.78 eV with a barrier of 0.88 eV. The barrier to diffusion to a second subsurface layer was calculated to be 0.52 eV. Greeley and Mavrikakis also showed that increasing the coverage of hydrogen had an initial cooperative effect, that is, that binding energies increased between 0 and 0.5 monolayers (ML) of hydrogen. Above 0.5 ML, the binding energies began to decrease. The calculations also indicated that high pressure of H_2 would be required to force the hydrogen to go subsurface.

Watson et al.[16] compared hydrogen adsorption on the three metals Pt, Pd and Ni and for Ni(111) calculated binding energies in close agreement to those later obtained by Greeley

and Mavrikakis. In a similar fashion, Paul and Sautet[17] analyzed the density of states for Pd and Ni surface hydride systems and found that relative to Pd, the Ni-H interaction is substantially stronger at the hcp site due to overlap of the Ni sp-band with the hydrogen s orbital.

A few in situ studies of hydrogen on metal electrodes exist, for example, in situ infra-red, but none on the Ni(111) surface. This is in part due to the difficulty of preparing an inert Ni(111) surface for in situ observation. In situ studies on Pt and Pd, however, show hydrogen uptake (use refs). Jaksic[18] reported a peak in the cyclic voltammetry current profile for desorption of hydrogen at 0 V NHE in pH 13 solution.

Progress towards modeling in situ environments has been made in the area of high coverage water bilayer structures on metal surfaces. Bilayer models, first expounded by Doering and Madey[19] predict the formation of ordered puckered hexagonal structures of water in a $\sqrt{3}x\sqrt{3}$ pattern atop the (111) lattice. The Ni(111)/bilayer mismatch, however, introduces a comparatively large compressive strain of about 4% upon the hydrogen bonded water structure. For this reason, water bilayers on nickel have been demonstrated to be only weakly binding, forming partially dissociated overlayers rather than inert bilayer structures[20]. The structure of water clusters on Ni(111) have been shown to be hexagonal at low coverage[21], and non-commensurate with the Ni(111) atomic positions. Siepmann and Sprik[22] also contest the bilayer structure, showing through molecular dynamics simulations that the ordered hexagonal bilayers give way to dynamically disordered groupings of four-, five- and six-membered arrangements. It should be noted that there is a significant controversy in the literature regarding the structure of water bilayers on noble and transition metals (see for example references [23], [24] and [25]). The

controversy arises primarily due to the extreme sensitivity of water structure to slight changes in the strength of metal-water versus water-water interactions as well as the lattice parameter of the metal.

Filhol and Neurock[26] used a novel method for calculating the electrochemistry of hydrogen at a model Pd(111)/H_2O interface using first principles techniques. Hydrogen adsorption was demonstrated to be dependent on the electrochemical potential, even at zero Kelvin, with an equilibrium potential for adsorption at +0.55 V NHE. Filhol's work remains the most developed theoretical exposition of hydrogen on an electrode to date.

In this paper we consider the *in situ* chemistry of hydrogen at the Ni(111)/H2O interface using two separate models. In the first model we adopt the minimal bilayer model of water on the Ni(111) surface. Although bilayers have been demonstrated to be unlikely candidates for the exact structure of water at the surface they provide an excellent first model for approaching bulk solvation. In this way we can assess the affect of an aqueous environment upon the binding energies modeled by previous UHV studies. Secondly we apply Filhol's method, using a bulk-propagated bilayer model of the solvent, to model the electrochemical dependence of hydrogen adsorption and absorption. We have also extended Filhol's method to allow the diffusion of interacting species to and from the model system via the inclusion of energetic terms for the chemical potential of such species. Extrapolations of energetic data obtained at zero Kelvin make it possible to model the thermodynamics at ambient and elevated temperatures.

Computational Details

Hydrogen mobility and uptake at the Ni(111)/H_2O interface were modeled using periodic gradient-corrected plane-wave density functional theory as implemented in VASP (the Vienna Ab initio Simulation Program)[27-29]. The metal/water interface was examined by carrying out calculations using a periodic slab architecture where the metal surface is defined by three layers of metal atoms and the solution phase placed between the metal slab with a density close to that of liquid water. Previous work indicated that increasing the slab width to five layers made no significant changes to the structural and energetic parameters. Ionic and core interactions were modeled via relativistic Vanderbilt ultra-soft pseudopotentials[30], and energy cut-offs of 396 eV were used. A super-cell was constructed containing 27 Ni atoms (three Ni(111) planes containing nine atoms in each plane) and either 6 water molecules for the bilayer studies or 24 water molecules (4 bilayers) for the bulk solvation model. Calculations performed using the RPBE functional[31,32] and a 3x3x1 Monkhorst-Pack k-point mesh[33] was used. Electronic energies were converged to within 0.1 meV. The calculated magnetic moment of Ni was $0.64\mu_B$ *versus* $0.61\mu_B$ for bulk Ni[34].

A conjugate gradient steepest descent method[35] was then used to determine the local minimum in the atomic structure to within 1.0 meV. Water bilayers were constructed following the theory of Doering and Madey[19] (see Figure 1). The equilibrium structure of the bulk solvation model corresponds with that of ferroelectric ice, leading to two uniquely oriented Ni(111)/H_2O interfaces within the super-cell (the oxidizing and reducing faces of Figure 2). Hydrogen was placed at various sites in and on top of the

metal electrode and the atomic coordinates again relaxed using the conjugate gradient method.

Electrochemical potentials were calculated using the method of Filhol and Neurock[26], whereby the potential is referenced to the free electron via the construction of a supercell containing a layer of free space some distance from the surface. In this way a vacuum electrode is introduced and *absolute* potentials may be determined. The potential of non-neutral slabs is determined by the creation of a second reference electrode at the midpoint of the aqueous phase. Further details of this double reference system are given in a previous publication[36]. Electrochemical potentials are then referred to the standard hydrogen electrode following Trasatti[37].

Gibb's free energies were estimated for solution species using the tables provided by Criss and Cobble[38-40]. Entropic and zero point vibrational terms were calculated directly for surface, atomic and molecular species using models for vibrational, translation and diffusional degrees of freedom derived from harmonic frequency calculations in VASP, and standard recipes from statistical mechanics[41].

Results and Discussion

Hydrogen beneath a water bilayer on Ni(111):- The binding energies of hydrogen at various adsorption and absorption sites beneath a water bilayer as shown in Figure 1 were calculated and are presented in Table 1. The coverage of hydrogen is 0.11 ML, corresponding to one hydrogen per 3x3 cell. Binding energies are given with reference to molecular hydrogen, and therefore correspond to the energy to dissociatively adsorb H_2 on the surface per hydrogen atom. We find that dissociative adsorption of H_2 at 1 atm

only occurs when hydrogen binds at the two three-fold hollow sites, which are near degenerate (-0.19 and -0.22 for fcc and hcp respectively). These binding energies are 0.3 eV lower than those obtained by Christmann et al. for the 0.5 ML (2x2)-2H structure, and between 0.3 and 0.4 eV lower than those obtained in previous computational studies of the 0.25 ML (2x2)-H surface[11,16]. We attribute our lower values to a coverage effect, rather than to the effect of the bilayer, since the binding energy of 0.11 ML of hydrogen at the hcp site in vacuo was calculated in this study to be -0.24 eV, i.e. the effect of the bilayer is less than 0.02 eV. A second calculation at 0.5 ML (the experimentally observed (2x2)-2H structure[2]) in vacuo gave the same binding energy for hydrogen (-0.64 eV) as that reported previously[11,16]. The vertical displacements of hydrogen from the surface (Table 1) are also in agreement with those given in previous studies[11,16].

The relative binding energies are close to those reported in previous studies. Absorption from the fcc surface site into the octahedral sub-surface site is endothermic by at least 0.59 eV. Adsorption to the tetrahedral site from the hcp position is endothermic by 0.74 eV. In the absence of defects and traps, hydrogen absorption into pure nickel from the gas has been shown to be endothermic[10]. Greeley and Mavrikakis[11] find, using DFT studies *in vacuo* (without the presence of a water bilayer), that absorption to the octahedral interstitial is endothermic by 0.71 eV and absorption to the tetrahedral interstitial is endothermic by 0.83 eV, in reasonable agreement with values calculated here. At low pressures, therefore hydrogen will not absorb into the bulk. The collision-induced absorption study by Maynard et al.[13] confirms this, by showing that absorption can be induced collisionally by noble gas atoms of energies > 2.6 eV. Absorption in solution, however, is unlikely to involve such high energy collisions, and

hydrogen uptake on Ni(111) must occur at defect sites that enhance hydrogen transport. It is also possible that the expansion of the nickel lattice upon hydrogen absorption (the lattice constant increases from 3.52 to 3.73)[42] significantly improves the thermodynamics of absorption through this crystal face, an effect not modeled in the theoretical studies.

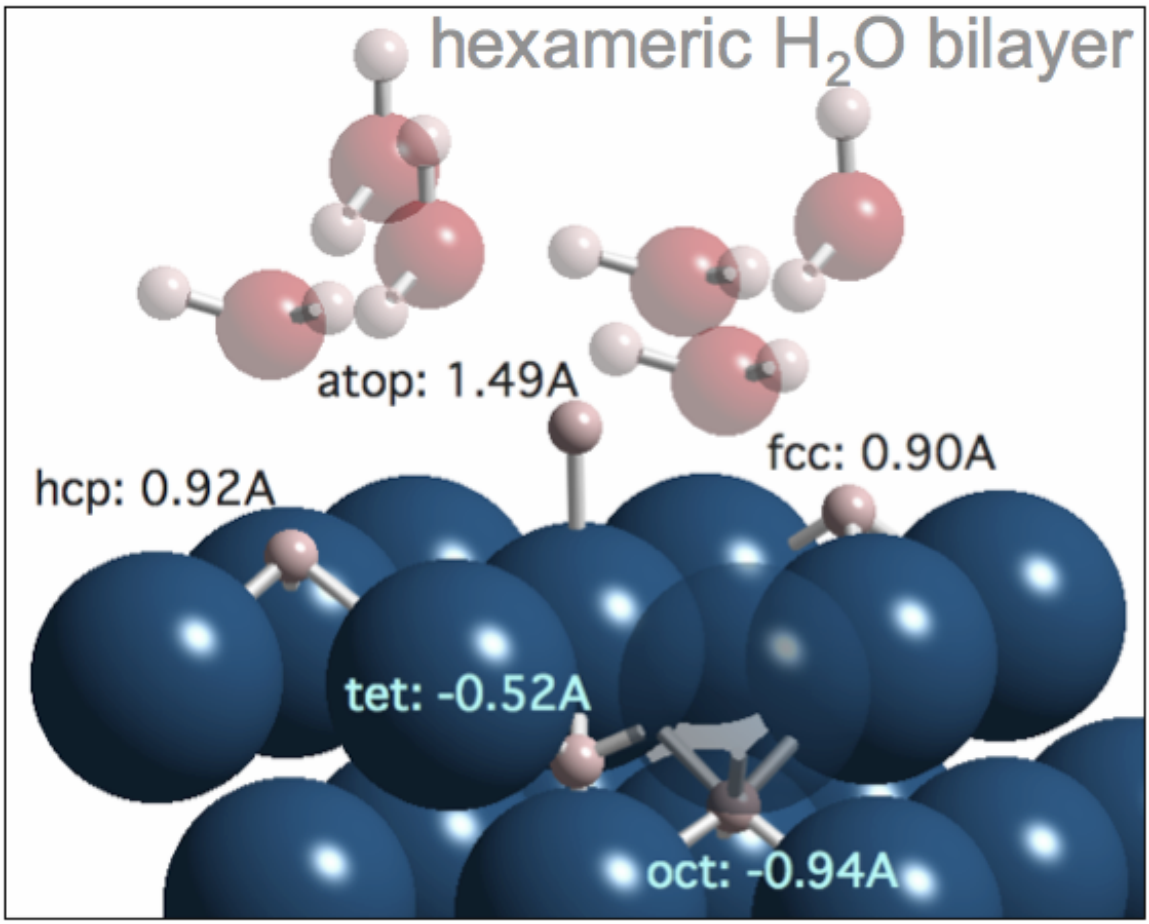

Figure 1. Various hydride phases beneath a H-up water bilayer on Ni(111)

Table 1. Binding energies, E_b, relative to molecular hydrogen, change in work-function, $\Delta\Phi$, and nickel-hydrogen bond distances, d(Ni-H), for the various hydride phases shown in Fig. 2.

	ATOP	FCC	HCP	OCT	TET
E_b (eV)	0.23	-0.19	-0.22	0.40	0.52
$\Delta\Phi$ (eV)	-3.39	-3.41	-3.39	-3.37	-3.38
d(Ni-H)	1.49	0.90	0.92	-0.94	-0.52

The change in work function induced by the hydrogen/bilayer environment, $\Delta\Phi$, is perturbed only slightly from the change induced by the bilayer alone (-3.40 eV). The water bilayer apparently screens any effect of the hydrogen upon the work function of the metal. Under UHV conditions, for example, Hammer et al.[12] found that hydrogen induced a 0.17 eV shift in the work function. A pH-dependence of the potential of zero charge of a Ni/H_2O solution was observed by Kheifets and Krasikov[43]. This latter result is more likely due to the change in surface composition and morphology occurring as a function of pH, as hydroxides, hydrides and oxides form on the surface, rather than a change due to the extent of hydrogen adsorption. The presence of a water bilayer in our simulation (not present in the UHV experiments) evidently dominates the work function change and screens the effect of the hydrogen atom on the surface.

Ultimately the results of the bilayer study suggest that the presence of a water overlayer does not affect the binding energy or geometry of hydrogen on the Ni(111) surface, except to screen the induced change in work function. Consequently we anticipate that the (2x2)-2H structure observed by Christmann et al.[2] is also relevant to the chemistry of hydrogen at the Ni(111)/H_2O interface.

Hydrogen at the reducing Ni(111)/H_2O interface:- In Figure 3 we have presented the binding energy for hydrogen on Ni(111) beneath a saturated water environment as a function of electrochemical potential. A sample geometry is shown in Figure 2. As in the bilayer study, we see that the hcp and fcc sites are preferred. The nature of binding at these sites is clearly different. While the binding energy at the fcc site is essentially independent of potential, binding at the hcp site becomes more favorable at negative

potentials. This implies that adsorption at the hcp site involves partial electron transfer, most likely due to the unique interaction of hydrogen with the nickel sp-band that this site allows[17]. The magnitude of electron transfer can be estimated from the slope of the curve in Figure 3. Binding at the subsurface tetrahedral site, for example, releases 0.42 and is therefore slightly oxidizing. Binding at the hcp and octahedral sites, on the other hand, is reducing with electron gains of 0.21 e and 0.25 e, respectively. Adsorption of hydrogen atoms at the fcc and atop sites is electroneutral.

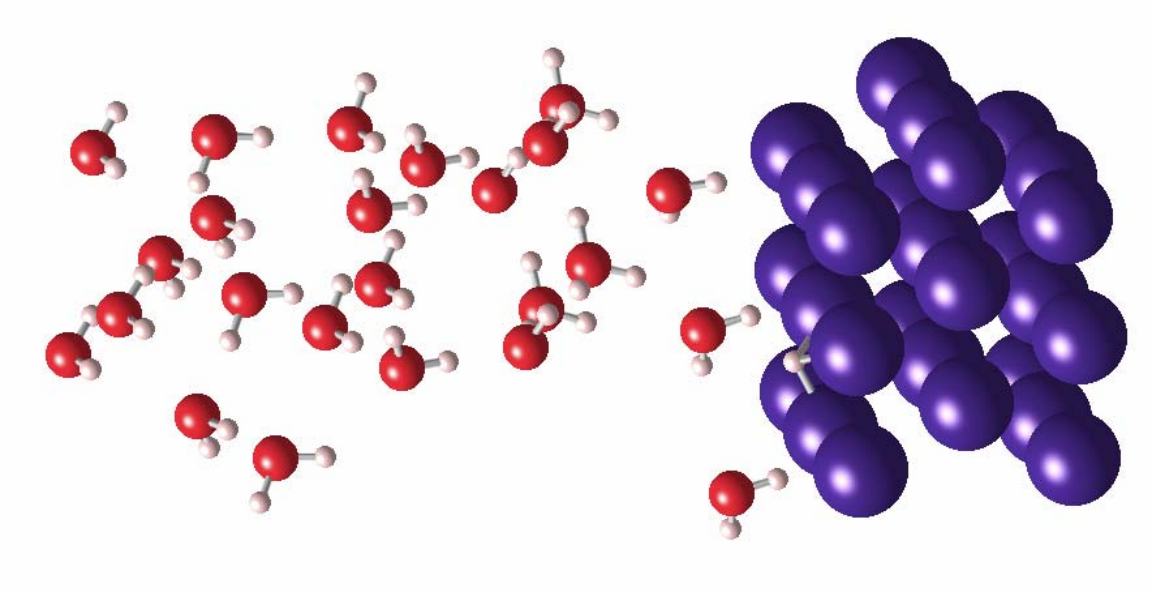

Figure 2. Ni-H supercell. H adsorbs in the hcp hollow site, beneath the cathodically oriented (H-down) water monolayer.

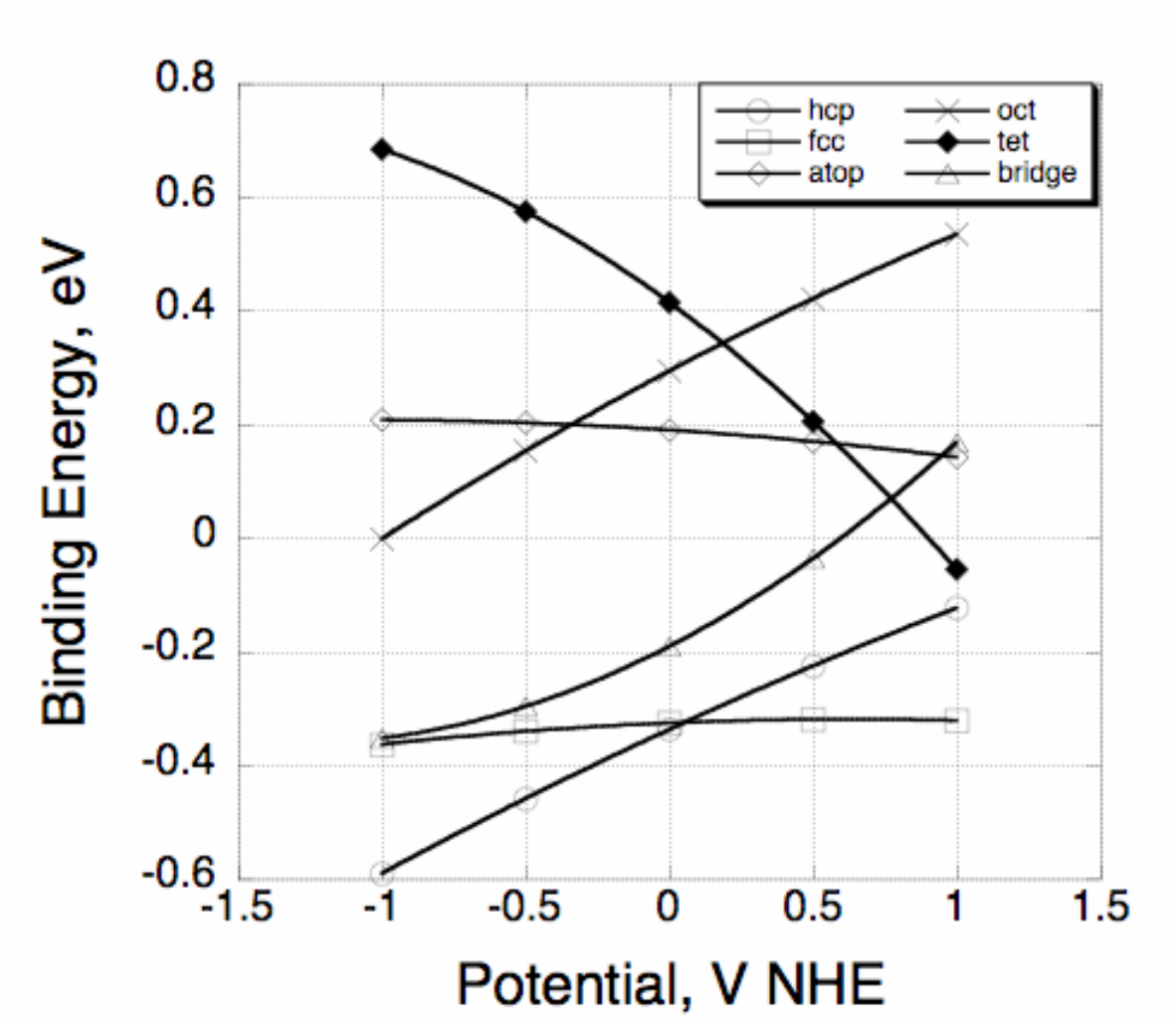

Figure 3. Binding energies per hydrogen atom relative to molecular hydrogen for hydrogen at surface (atop, hcp and fcc), and sub-surface (tet, oct) sites on and in Ni(111).

These electrons are pooled from or released to the substrate reservoir, either in the form of electron transfer from/to an external electrode, or by local surface fluctuations in the metal (Scheme 1). If electron transfer *does not occur* then there should be no dependence of the adsorption processs upon potential, and the binding energies for hydrogen on the substrate should be constant, as is the case for hydrogen at the fcc site. The use of partial charge transfer mechanisms during the formation of chemisorbed species and

intermediates has been discussed by Lorenz[44]. Vargas and Christensen[45] report partial charge transfer from nickel to a hydrogen atom bound at the octahedral site of between 0.18 and 0.48 electrons depending on the electron-counting method used, a range which is not in disagreement with the 0.25 e observed here.

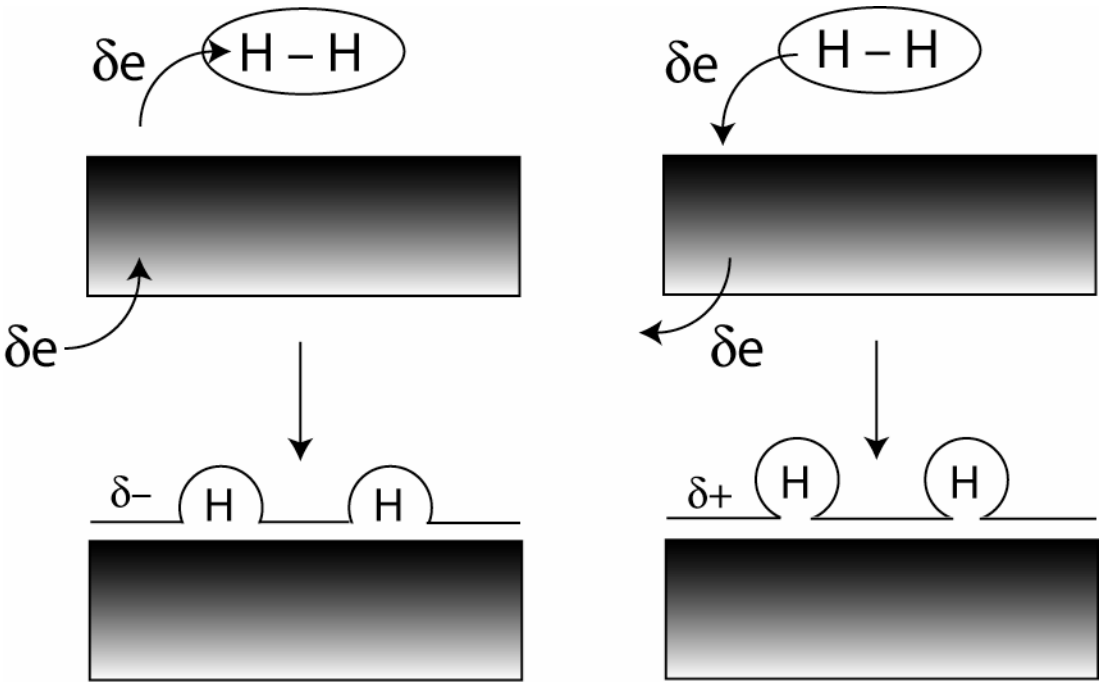

Scheme 1. A schematic depicting how partial electron transfer upon adsorption can lead to negative (as in the case of hcp, left) or positive (as in the case of atop, right) local surface charge densities.

These effects are also noticeable in the variation of Ni-H distance from the surface with changes in the electrochemical potential (Figure 4, open circles – hcp, filled circles – fcc, open triangles - bridge). Hydrogen atoms at the fcc, hcp and bridging sites are repelled from the surface when the interface is anodically charged. The effect is greater by an

order of magnitude at the hcp and bridging sites, in agreement with the more strongly reducing behavior observed in Figure 3. Conversely, hydrogen atoms at the atop site are attracted to the surface by increasingly anodic potentials, a feature that is consistent with the weakly oxidizing nature of atop binding (Figure 4, filled triangles).

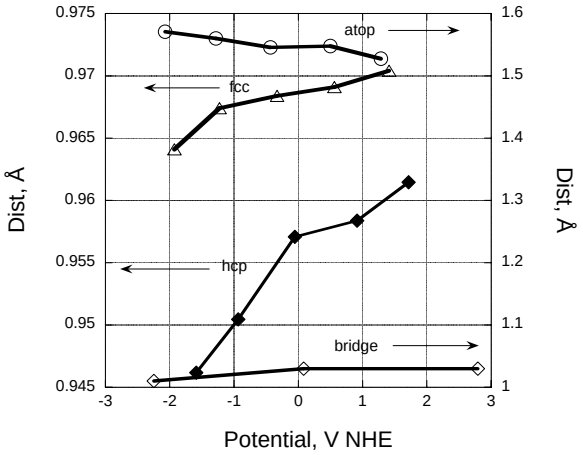

Figure 4. Variation in the Ni(111) surface - hydrogen distance (the height of hydrogen above the surface plane) at the hcp site as a function of electrochemical potential.

We can now calculate diffusion barriers as a function of electrochemical potential using the data in Figure 3. Hydrogen at the fcc site can diffuse to a neighboring hcp site via the nickel-nickel bridging site. From Figure 3 we see that the barriers range from 0 through to 0.3 eV. For hydrogen crossing from the hcp to fcc site the barrier is always close to 0.2 eV. For the reverse pathway, however, the barrier is 0.0 eV at -1 V NHE at 0.3 eV at +1 V NHE. This is indicative of the charge transfer occurring when the diffusion is performed at a constant potential. The barriers also suggest that at negative potentials hydrogen is trapped in the hcp site, whereas at potentials close to 0 V NHE there is an even distribution of hydrogen between sites.

The (111) surface of nickel is known to absorb atomic hydrogen under high pressures of H_2, or other colliding species[13]. In the presence of solvent, it is possible that collisions with solvent molecules and/or thermal agitation may cause hydrogen to absorb into the substrate. Absorption under the saturated water environment remains endothermic, becoming less so as the potential becomes cathodic. The absorption energy is 0.58 eV at -1.0 V NHE and 0.62 eV at 0.0 V NHE (Figure 3). Higher coverages and a forcing chemical potential for hydrogen are required to activate the absorption pathway, as noted by Greeley and Mavrikakis[11]. The low affinity of Ni(111) for absorption is supported by Huang and Raibeck, who performed kinetic Monte Carlo studies of hydrogen absorption into a nickel nanoparticle containing (100), (110), (111) steps in vacuo. For temperatures below 1000 K they find that hydrogen penetrates into the subsurface primarily at the defect (edge) suites, and to a lesser extent vias the (100) surface. The decreased corrugation of the (110) and (111) surfaces make them essentially close to hydrogen absorption except at temperatures greater that 1000 K.

While we have mapped the energetics of hydrogen bound to Ni(111) over the potential range from -1 V NHE through to +1 V NHE, it is likely that the relevant potential range of our predictions is much smaller. At cathodic potentials bulk nickel hydride, $NiH_{0.5}$, will form, with different lattice constants and chemical composition to the ideal Ni(111) surface presented herein. At anodic potentials β-$Ni(OH)_2$ and NiO are produced. Thus the binding of hydrogen to nickel here is only relevant to the small pH-potential window in which metallic nickel is inert to these major phase changes[46,47].

Hydrogen sorption at ambient and elevated temperatures:- The ab initio results presented thus far apply only to surface states at 0 K. In this section we calculate binding energies at ambient (298 K) and elevated (600 K) temperatures. We first consider binding energies relative to the molecular hydrogen, that is, the energy of reaction for:

H_2 (g) → 2H* [1]

We assume that molecular hydrogen occupies only vibrational, rotational and translational degrees of freedom, and that the adsorbed species occupies only vibrational and diffusional degrees of freedom. Vibrational degrees of freedom are calculated for a surface and subsurface phase of hydrogen on Ni(111). The frequencies, zero-point energies and entropies are given in Table 2. Entropic and zero-point effects were also calculated for adsorbed hydrogen at a cathodic potential (–1.30 V NHE). We see that although there are slight changes in the geometry of the adsorption system at these potentials (Figure 4) the entropic terms are equal to within 0.01 kJ/mol (or $1x10^{-4}$ eV). We therefore apply the same thermodynamic extrapolations derived at zero charge (0.23 V NHE) to the energies of the systems at all potentials within the range considered (–1.5 to +1.5 V NHE).

Adsorbed hydrogen atom may also occupy diffusional degrees of freedom. We calculate the diffusion barrier from one three-fold hollow site to another via the bridging site between two nickel atoms. The energy barrier for this is 0.2 eV as estimated from Figure 4. We approximate the partition function for diffusion by taking the following equation for a diffusion over a model sinusoidal potential[48]:

$$q_{xy} = \frac{\pi E_D}{\theta kT} e^{-E_D/kT} I_0^2\left(\frac{E_D}{2kT}\right)\left(1-\exp\left(-\left[\frac{2h^2}{ma_x^{\,2}E_D}\right]^{1/2}\frac{E_D}{2kT}\right)\right)^{-2} \quad [2]$$

Here θ is the coverage, m is the mass of the particle, a_x is the distance between neighboring hollow sites, and E_D is the diffusion barrier. The entropic contribution due to diffusion is 27.8 J/mol/K at 300 K and 31.4 J/mol/K at 600 K (Table 3).

We estimate the diffusional entropy of absorbed hydrogen in a similar way, using the *ab initio* barrier for subsurface diffusion calculated by Greeley and Mavrikakis[11]. Entropies of absorbed hydrogen at 300 K and 600 K are also given in Table 3.

Table 2. Frequencies, and zero point energies and entropic contributions to hydrogen adsorption (fcc) and absorption (oct) phases on Ni(111), and molecular hydrogen

H binding site	Frequency, x10^{13} Hz	ZPVE, kJ/mol	TS (300 K)	TS (600 K)
HCP (–0.3 V NHE)				
V_1	3.45	6.89	0.065	1.26
V_2	2.52	5.04	0.225	2.25
V_3	2.39	4.77	0.268	2.45
Total		16.7	0.56	5.96
HCP (–1.6 V NHE)				
V_1	3.42	6.83	0.068	1.28
V_2	2.51	5.00	0.231	2.28
V_3	2.43	4.85	0.254	2.39
Total		16.7	0.55	5.95
OCT (–0.2 V NHE)				
V_1	2.51	5.00	0.230	2.28
V_2	2.26	4.52	0.316	2.66
V_3	2.17	4.33	0.356	2.82
Total		13.9	0.902	7.74
H_2^{*exptl} (1 atm)	0.12	0.260	0.00	0.00

Table 3. Overall entropic contributions from vibrational, surface diffusional and translational degrees of freedom (terms given in kJ/mol).

	TS_{vib}		TS_{diff}		TS_{trans}		TS_{total}	
	300 K	600 K	300 K	600 K	300 K	600 K	300 K	600 K
Hcp	0.56	5.96	8.33	18.8	-	-	8.89	24.8
Oct	0.90	7.74	8.06[a]	16.9[a]	-	-	8.96	24.6
$H_{2(g)}$	0.00	0.00	3.81[b]	11.10[b]	35.4	79.2	39.2	90.3
$H^+_{(g)}$	-	-	-	-	34.5	77.4	34.5	77.4

[a]Diffusion to neighboring subsurface sites has been calculated based on sub-surface diffusion barrier estimated from Greeley and Mavrikakis[11].

[b]Rotational entropy calculated from statistical mechanics

The resulting plot of free energies as a function of potential is given in Figure 5. Hydrogen preferentially desorbs at anodic potentials. This is due to the loss of partial charge density occurring when hydrogen at the surface associates to form H_2. Desorption occurs at potentials greater than 0.7 V, 0.0 V and -1.3 V NHE at temperatures of 0 K, 300 K, and 600 K respectively. Increasing the temperature therefore forces the desorption of H_2 to lower and lower potentials. At 300 K, for example, hydrogen will be surface bound on the ideal Ni(111) electrode, rather than desorbing H_2 at potentials cathodic of the normal hydrogen electrode – i.e. molecular hydrogen evolution is stifled by preferential hydrogen adsorption. At 600 K this is not the case, and H_2 will bubble off the surface for potentials between 0 V NHE and -1.3 V NHE. At potentials greater than 0 V NHE, hydrogen will desorb to $H^+_{(aq)}$ as the following section shows.

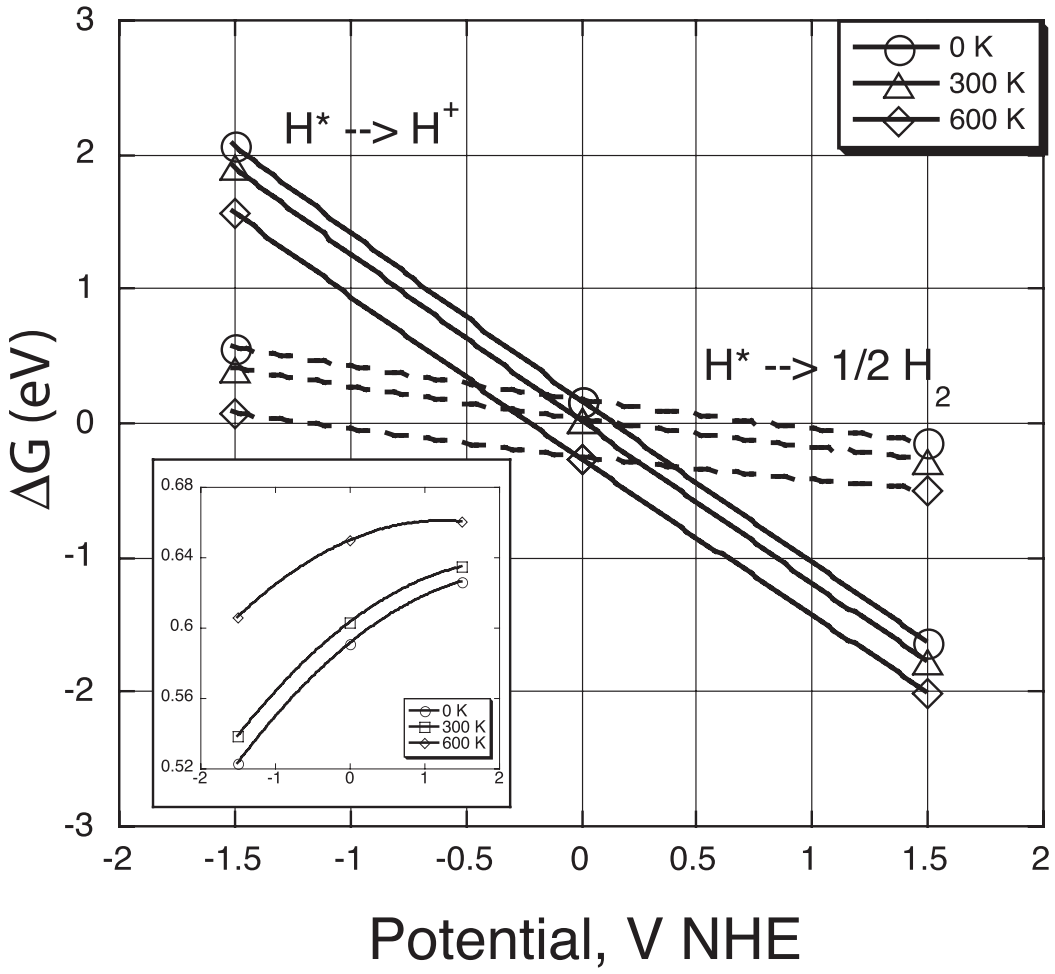

Figure 5. Desorption energies at 0 K, 300 K, and 600 K for adsorbed hydrogen to (a) the aqueous proton at 1 M concentration, (b) molecular hydrogen at 1 atm, and (c-inset) the octahedral subsurface state.

The following thermodynamic cycle allows us to calculate the binding energy of surface hydrogen relative to $H^{+}_{(aq)}$, by way of the readily calculable atomic gaseous hydrogen:

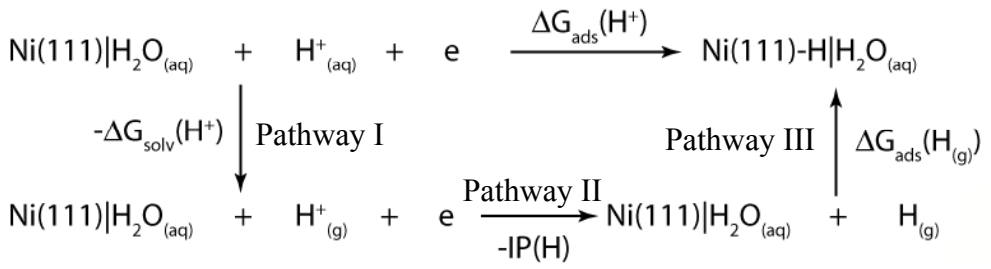

Scheme 2.

The free energy, $-\Delta G_{solv}(H+)$, is averaged over results taken from the literature[38-40,49-52]. At 300 K we use the value 1080 kJ/mol and at 600 K we use 970 kJ/mol, with an uncertainty of 30 kJ/mol. IP(H), the ionization potential of hydrogen, is adjusted for the system potential via the electrochemical potential of the electron:

$$IP = E(H^+) + e\mu_e - E(H) \qquad [3]$$

The chemical potential of the electron on the hydrogen scale may be determined from:

$$\mu_e = -V_{abs}^{NHE} - V \qquad [3.9]$$

V_{abs}^{NHE} is the absolute potential of the H_2/H^+ hydrogen reference electrode, which may be taken as 4.6±0.2 V (at STP) as averaged from a variety of experimental and theoretical measurements[37,53-55]. V is the arbitrary potential applied to the system with reference to the NHE scale. Because, in this study, we require the absolute potential at a variety of temperatures (0 K, 300 K, and 600 K), we calculate our own value using a Born cycle equivalent to that used by Llano and Eriksson[54]. We calculate V_{abs}^{NHE} as 4.51, 4.67 and 5.63 at 0 K, 300 K and 600 K respectively.

Entropic terms for gaseous atomic hydrogen are provided in Table 3. These entropic terms coupled with the difference in energy of the adsorbed phase, the Ni(111)/H2O interface without hydrogen and an isolated hydrogen atom comprise the term $\Delta G_{ads}(H)$.

The resulting plot of desorption energies as a function of potential is shown in Figure 5. As this is a one-electron process, unlike desorption to H_2, there is a strong dependence of aqueous desorption on the electrochemical potential. Desorption to H^+ is an oxidizing process, becoming more favorable at anodic binding potentials. The slope of the binding energy curve is not exactly one, in accordance with the observations regarding partial electron transfer noted previously. Equilibrium potentials for the half-cell reaction, with a standard H^+ concentration of 1 M:

$$H^+ + e \rightarrow H^* \qquad [4]$$

are 0.2 V, 0.0 V and -0.3 V NHE at 0 K, 300 K and 600 K. This gives the interesting result that the hydrogen electrode reaction is in equilibrium with hydrogen adsorption at 300 K.

The desorption of hydrogen onto Ni(111) becomes increasingly favored at high temperatures. This observation may be primarily attributed to the large loss of entropy of the solvated proton occurring upon adsorption, compared to the small gain in entropy obtained as the adsorbed hydrogen atom is heated. This effect is magnified as the temperature increases. Gleaning the appropriate values from Tables 2 and 3 we find that the leading entropic terms accounting for the endothermic shift in energies from 0 K to 300 K are the loss of proton mobility (+34.5 kJ/mol) and the shift in the H_2/H+ reference electrode (+15.4 kJ/mol). The smaller exothermic effects result from the gain in surface mobility (–9.6 kJ/mol) and the desolvation entropy (–30 kJ/mol). As we move from 300 K to 600 K similar effects occur: +42.9, +92.5, –17.8 and –110 kJ/mol for the loss of proton mobility, H_2/H^+ shift, surface mobility and desolvation entropy respectively.

Absorption is endothermic and becomes increasingly so at higher temperatures (inset, Figure 5). The Gibb's free energy of absorption ranges from between 0.52 and 0.67 eV depending upon the temperature and potential. There is no equilibrium potential for hydrogen absorption (it is essentially an electroneutral process). The endothermic dependence upon increasing temperature may be attributed to the greater mobility of surface hydrogen compared to the sub-surface state, as seen in the entropies presented in Table 3. We may therefore conclude that there is no absorption occurring through the ideal terraces sites on a Ni(111) surface, and that any absorption of hydrogen must be occurring through defect sites such as grain boundaries, step-edges, surface vacancies, or more corrugated surface planes (such as the (110) plane). The investigation of such defects, and the consideration of other surface planes should be considered crucial for the further understanding of hydrogen electrochemistry on nickel substrates.

By introducing an energetic term for the chemical potential of H^+ we can create pH-potential phase diagrams for hydrogen on the surface, in analogy with the Pourbaix diagrams for bulk phases[46,47]. Surface phase diagrams for the H^+, H* and H_2 phases of hydrogen at 300 K are presented in Figure 6.

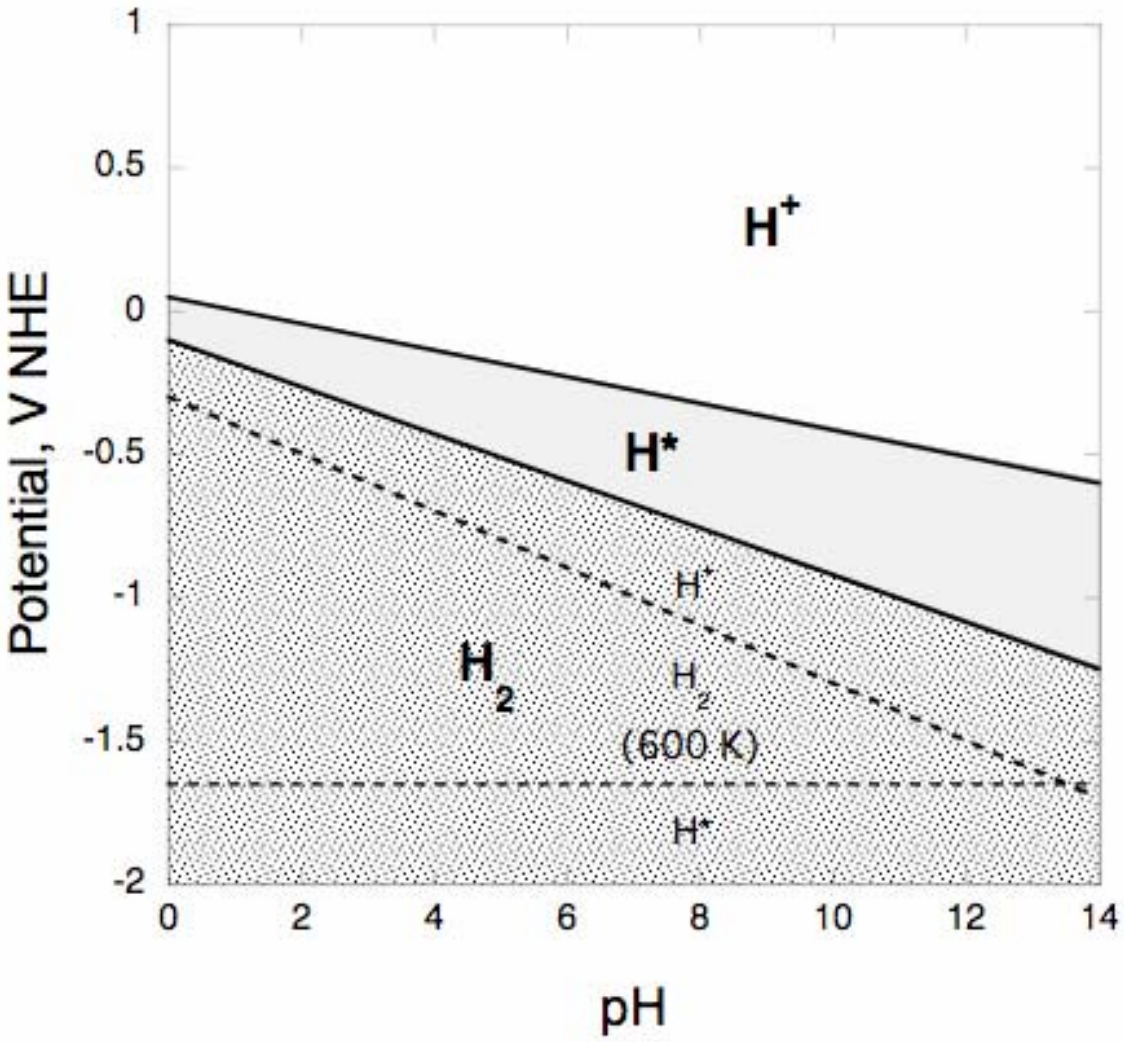

Figure 6. Phase diagram for aqueous ionized hydrogen, $H^{+}_{(aq)}$, surface adsorbed hydrogen, H*, and molecular hydrogen, H_2, plotted versus pH and potential (shaded regions- 300 K, dashed lines- 600 K).

The results displayed in Figure 6 imply that hydrogen evolution occurs via two different mechanisms depending on the temperature. At 300 K molecular hydrogen evolution proceeds via the electrochemical reaction between an adsorbed hydrogen atom and a proton in solution:

$H^* + H^+ + e \rightarrow H_2$ [4]

Suzuki, Yamada and Itaya[56] observe hydrogen evolution on Ni(111) at –0.16 V NHE in a pH 3 environment. This potential is between the -0.08 V calculated at the same pH using Figure 6 for hydrogen adsorption and the -0.34 V for hydrogen evolution.

At 600 K, on the other hand, there is no intermediate region where H* is most stable. Rather, H^+ electrochemically begins to adsorb on the surface as H* from which H_2 is immediately evolved from the combination of two adsorbed hydrogen atoms:

$H^+ + e \rightarrow [\ H^*\ ] \rightarrow \frac{1}{2}\ H_2$ [5]

Since H_2 evolution from adsorbed hydrogen was found previously to be weakly oxidizing, at potentials lower than -1.65 V NHE, molecular hydrogen dissociates to form H* on the surface.

Conclusions

The results of this study provide significant insight as to the electrochemical behavior of hydrogen on an immersed Ni(111) electrode at constant potential. In particular we find that partial electron transfer is required to maintain a constant potential environment. For example, the dissociation of molecular hydrogen at the Ni/H_2O interface has been shown to be partially reducing such that, at ambient temperatures and cathodic potentials hydrogen will prefer to remain adsorbed rather than leaving the surface as H_2. Evolution of H_2 may instead be induced by the reaction between a desorbing hydrogen atom and a reduced proton in solution. This is likely to occur as higher coverages of hydrogen are maintained.

At constant potential hydrogen absorption from the surface fcc site through to the octahedral site is also reducing, implying that a net gain in electronic charge occurs, either from the local surface charge density, or from another electrode. This also suggests that hydrogen uptake should be noticeable as a peak in cyclic voltammetry, and that hydrogen absorption will become less endothermic at cathodic potentials. Hydrogen uptake is always endothermic on the ideal terraces of Ni(111), however, in the range of -1.5 through to 1.5 V NHE, and therefore any hydrogen uptake occurring on Ni(111) surfaces must be occurring at either step sites, defect sites, or grain boundaries.

References

1. S. A. Attanasio and D. S. Morton, *11th Intl. Conference on Environmental Degradation of Materials in Nuclear Systems*, (2003).
2. K. Christmann, O. Schober, G. Ertl and M. Neumann, *J. Chem. Phys.*, **60**, 4528 (1974).
3. D. M. Kolb, *Angew. Chem. Int. Ed. Engl.*, **40**, 1162 (2001).
4. D. M. Kolb and L. A. Kibler, *Zeit. Phys. Chem.*, **217**, 1265 (2003).
5. A. Bewick and K. Kunimatsu, *Surf. Sci.*, **101**, 131 (1980).
6. T. Iwasita and F. C. Nart, *Prog. Surf. Sci.*, **55**, 271 (1997).
7. J. Kunze, V. Maurice, L. H. Klein, H.-H. Strehblow and P. Marcus, *Corrosion Sci.*, **46**, 245 (2004).
8. B. J. Cruickshank, D. D. Sneddon and A. A. Gewirth, *Surf. Sci. Lett.*, **281**, 308 (1993).
9. G. Niaura, *Electrochim. Acta*, **45**, 3507 (2000).
10. M. Wilms, P. Broekmann, C. Stuhlmann and K. Wandelt, *Surf. Sci.*, **416**, 121 (1998).
11. J. Greeley and M. Mavrikakis, *Surf. Sci.*, **540**, 215 (2003).
12. L. Hammer, H. Landskron, W. Nichtl-Pecher, A. Fricke, K. Heinz and K. Muller, *Phys. Rev. B.*, **47**, 15969 (1993).
13. K. J. Maynard, A. D. Johnson, S. P. Daley and S. T. Ceyer, *Faraday Discuss.*, **91**, 437 (1991).
14. S. Wright, J. F. Skelly and A. Hodgson, *Faraday Discuss.*, **117**, 133 (2001).
15. H. Yanagita, J. Sakai, T. Aruga, N. Takagi and M. Nishijima, *Phys. Rev. B.*, **56**, 14952 (1997).
16. G. W. Watson, R. P. K. Wells, D. J. Willock and G. J. Hutchings, *J. Phys. Chem. B.*, **104**, 6439 (2000).
17. J.-F. Paul and P. Sautet, *Surf. Sci.*, **356**, 403 (1996).
18. M. M. Jaksic, J. Brun, B. Johansen and R. Tunold, *Int. J. Hydrogen Energy*, **20**, 265 (1995).
19. D. L. Doering and T. E. Madey, *Surf. Sci.*, **123**, 305 (1982).
20. A. Michaelides, A. Alavi and D. A. King, *Phys. Rev. B.*, **69**, 113404 (2004).
21. M. Nakamura and M. Ito, *Chem. Phys. Lett.*, **384**, 256 (2004).
22. J. I. Siepmann and M. Sprik, *J. Chem. Phys.*, **102**, 511 (1995).
23. S. Meng, E. G. Wang, C. Frischkorn, M. Wolf and S. Gao, *Chem. Phys. Lett.*, **402**, 384 (2005).
24. S. Meng, L. F. Xu, E. G. Wang and S. Gao, *Phys. Rev. Lett.*, **89**, 176104 (2002).
25. P. Fiebelman, *Phys. Rev. Lett.*, **91**, 59601 (2003).
26. J.-S. Filhol and M. Neurock, *(unpublished)*.
27. G. Kresse and J. Furthmuller, *Phys. Rev. B.*, **54**, 11169 (1996).
28. G. Kresse and J. Furthmuller, *Comput. Mater. Sci.*, **6**, 15 (1996).
29. G. Kresse and J. Hafner, *Phys. Rev. B.*, **47**, 558 (1993).
30. D. Vanderbilt, *Phys. Rev. B.*, **41**, 7892 (1990).
31. J. P. Perdew, K. Burke and M. Ernzerhof, *Phys. Rev. Lett.*, **77**, 3865 (1996).
32. J. P. Perdew, K. Burke and M. Ernzerhof, *Phys. Rev. Lett.*, **80**, 891 (1998).
33. H. J. Monkhorst and J. D. Pack, *Phys. Rev. B.*, **13**, 5188 (1976).

34. I. M. L. Billas, A. Chatelain and W. A. de Heer, *Science*, **265**, 1682 (1994).
35. M. C. Payne, M. P. Teter, D. C. Allan, T. A. Arias and J. D. Joannopoulos, *Rev. Mod. Phys.*, **64**, 1046 (1992).
36. C. D. Taylor, S. A. Wasileksi, J. W. Fanjoy, J.-S. Filhol and M. Neurock, *Phys. Rev. B. (submitted)* (2005).
37. S. Trasatti, *Electrochim. Acta*, **36**, 1659 (1991).
38. J. W. Cobble, *J. Am. Chem. Soc.*, **86** (1964).
39. J. W. Cobble, *J. Am. Chem. Soc.*, **86**, 5390 (1964).
40. C. M. Criss and J. W. Cobble, *J. Am. Chem. Soc.*, **86**, 5385 (1964).
41. P. A. Rock (1983) Chemical Thermodynamics. University Science Books.
42. R. Juškėnas, A. Selskis and V. Kadziauskienė, *Electrochim. Acta*, **43**, 1903 (1998).
43. V. L. Kheifets and B. S. Krasikov, *Dok. Akad. SSSR*, **109**, 556 (1956).
44. W. Lorenz, *J. Phys. Chem.*, **95**, 10566 (1991).
45. P. Vargas and N. E. Christensen, *Phys. Rev. B.*, **35**, 1993 (1987).
46. B. Beverskog and I. Puigdomenech, *Corr. Sci.*, **39**, 969 (1997).
47. E. Deltombe, N. de Zoubov and M. Pourbaix (1974) Atlas of Electrochemical Equilibria in Aqueous Solution. M. Pourbaix (ed.) Houston, Texas: NACE.
48. R. I. Masel (1996) Principles of adsorption and reaction of solid surfaces. Wiley Interscience.
49. J. A. Mejias and S. Lago, *J. Chem. Phys.*, **113**, 7306 (2000).
50. M. D. Tissandier, K. A. Cowen, W. Y. Feng, E. Gundlach, M. H. Cohen, A. D. Earhart, J. V. Coe and T. R. Tuttle Jr., *J. Phys. Chem. A.*, **102**, 7787 (1998).
51. G. Hummer, L. R. Pratt and A. E. Garcia, *J. Phys. Chem.*, **100**, 1206 (1996).
52. T. F. Magnera, D. E. David and J. Michl, *Chem. Phys. Lett.*, **182**, 363 (1991).
53. J. O. M. Bockris, A. K. N. Reddy and M. Gamboa-Aldeco (2000) Modern Electrochemistry. Vol. 2A New York: Kluwer Academic/Plenum Publishers.
54. K. Llano and L. A. Eriksson, *J. Chem. Phys.*, **117**, 10193 (2002).
55. H. Reiss and A. Heller, *J. Phys. Chem.*, **89**, 4207 (1985).
56. T. Suzuki, T. Yamada and K. Itaya, *J. Phys. Chem.*, **100**, 8954 (1996).